DNA Helicase RepA: Cooperative ATPase Activity and Binding of Nucleotides†

Hai Xu,‡ Joachim Frank,§ Timo Niedenzu,‡ and Wolfram Saenger*,‡

Institut für Kristallographie, Freie Universität Berlin, Takustrasse 6, and Fritz-Haber-Institut, Max-Planck-Gesellschaft, Faradayweg 4-6, D-14195 Berlin, Germany

Received April 19, 2000; Revised Manuscript Received July 10, 2000

ABSTRACT: The steady-state kinetic parameters of the ATPase activity of the homohexameric DNA helicase RepA and the binding of the fluorescent analogue ϵADP to RepA have been studied. ssDNA stimulates RepA ATPase activity optimally at acidic pH 5.3−6.0. The sigmoidal kinetic curves in both the absence and presence of ssDNA show strong positive cooperativity for ATP hydrolysis, with oligonucleotides longer than 10mer optimal for ssDNA-stimulated ATPase activity. Fluorescence titrations show that, at 25 °C and in the absence of DNA, the binding of ϵADP to RepA is biphasic with three high ($K_1 = 1.54 \times 10^6$ M^{-1}) and three low ($K_2 = 4.71 \times 10^4$ M^{-1}) affinity binding sites differing by 30−40-fold in binding constants. In the absence of cofactors, RepA melts cooperatively at $T_m = 65.8 \pm 0.1$ °C and is more stable in the presence of ATPγS, $T_m = 68.1 \pm 0.2$ °C ($\Delta\Delta G$ 0.95 kcal/mol), than in the presence of ADP, $T_m = 66.5 \pm 0.1$ °C ($\Delta\Delta G$ 0.29 kcal/mol), indicating that the additional phosphate group in ATPγS has a significant influence on RepA structure. A model is proposed in which individual subunits of RepA sequentially and cooperatively perform a multistep ATP hydrolytic cycle.

DNA helicases are a large family of motor proteins with essential roles in key biological processes including DNA replication, repair and recombination, transcription, and translation (*1*, *2*). They unwind double-stranded DNA (dsDNA) to single-stranded DNA (ssDNA) intermediates using the chemical energy of nucleoside 5'-triphosphate (NTP) hydrolysis and are strictly processive, acting either in the 5' → 3' or in the 3' → 5' direction.

A growing number of helicase proteins which are involved in many aspects of metabolism in bacterial, viral, and eukaryotic systems have now been characterized in vitro. Several human diseases, including Bloom syndrome, *Xeroderma pigmentosum*, and Werner syndrome, are caused by defects in DNA helicases required for nucleotide excision repair (*3*−*5*). All DNA helicases for which the assembly state of the enzyme has been examined appear to function as oligomers, generally dimers or hexamers, thus providing multiple potential DNA binding sites, which are required for helicase function. The *Escherichia coli* DnaB protein (*6*, *7*), the bacteriophage T7 gp4 protein (*8*), the *E. coli* branch migration RuvB protein (*9*), and the *E. coli* transcription termination protein Rho (*10*) assemble into a hexameric ring, while the *E. coli* proteins Rep (*11*) and UvrD (*12*) (helicase II) have been characterized as dimers.

The replicative hexameric helicase RepA is encoded by the broad host range plasmid RSF1010, an 8684 base pair (bp) multicopy plasmid that can replicate in a wide variety of Gram-negative and also Gram-positive actinomyces (*13*). Three plasmid-encoded proteins, RepA, RepB', and RepC, exhibit RSF1010-specific helicase, primase, and initiator protein activities, respectively, and are essential to the replication of this plasmid. *E. coli* DNA gyrase, SSB (single-stranded DNA binding protein), and the production of dnaZ (γ subunit of DNA polymerase III holoenzyme) are also required for replication of plasmid RSF1010, while the bacterial RNA polymerase and the DnaA, -B, -C, -G, and -T proteins are not required (*14*). RepA is one of the smallest known homohexameric helicase enzymes with a total molecular mass of 180 kDa (*15*). It unwinds dsDNA in 5′ → 3′ polarity and prefers a tailed substrate with an unpaired 3′-tail mimicking a DNA replication fork. The RepA activity is fueled by ATP, dATP, GTP, and dGTP and less efficiently by CTP and dCTP, while UTP and dTTP are poor effectors. Optimal unwinding activity was found at a narrow pH range around 5.5 (*15*), similar to that observed for yeast *Saccharomyces cerevisiae* RAD3 helicase (*16*). Below pH 5.6 and at low salt concentration, the RepA hexamers aggregate and form tubular structures (*17*).

Crystal structure analyses of truncated domains of two hexameric helicases, DnaB (*18*) and T7 bacteriophage helicase−primase (*19*), have been reported. RepA is the first intact hexameric replicative DNA helicase whose three-dimensional structure is known in detail (at 2.4 Å resolution) (Niedenzu et al., in preparation). The RepA hexamer is pot shaped with a 17 Å wide central hole. The six ATP binding sites of RepA are each located at the interfaces between two adjacent monomers. They are defined by the consensus sequence for the P loop (*20*) ^{40}GAGKS^{44} and residues Asp140, Glu77, His179 (belonging to the same monomer), and Arg207 (from the adjacent monomer). The adenine base is found sandwiched between Arg254 of the same (in cis) and Tyr243 of the adjacent (in trans) monomer. All of the residues essential for triphosphate binding and hydrolysis in RepA are conserved in helicases and related enzymes utilizing NTP hydrolysis (*21*, *22*).

†This work was supported by an EC project, by DFG-Sonderforschungsbereich 344, and by Fonds der Chemischen Industrie.

* Corresponding author. Phone: +49-30-83853412. Fax: +49-30-83856702. E-mail: saenger@chemie.fu-berlin.de.

‡ Freie Universität Berlin.

§ Max-Planck-Gesellschaft.

10.1021/bi0008938 CCC: $19.00
Published on Web 09/08/2000

For helicase-catalyzed unwinding of dsDNA, NTP binding and hydrolysis are essential. The NTPs can function as switches that induce conformational changes necessary to promote DNA binding and release steps required for translocation of helicase along the DNA double helix (*23*). Until now, the molecular mechanism by which NTP binding and hydrolysis are coupled to DNA unwinding is poorly understood. It is a common feature of the hexameric helicases that the six potential nucleotide binding sites are nonequivalent and can be clearly distinguished as three high-affinity and three low-affinity binding sites, as found for DnaB helicase (*24*) and for transcription termination protein Rho (*25*). In bacteriophage T7 DNA helicase, only three high-affinity nucleotide binding sites per hexamer are observed, the low-affinity binding sites being nearly undetectable (*26*).

Although DNA helicase RepA has been characterized biochemically (*15*), detailed studies of its mechanism of NTP binding and hydrolysis activity are still in the early stages. It is clear, however, that understanding the interaction of RepA helicase with NTP and the regulatory role of NTP are crucial elements in further elucidating the DNA unwinding mechanism. For this reason, we investigated the steady-state kinetics and cooperativity of ATPase activity and employed fluorescence titration and CD experiments to further determine the properties of NTP binding; the results are described in this paper.

MATERIALS AND METHODS

Reagents and Buffers. All chemicals used in this study were of p.a. quality. Ammonium molybdate tetrahydrate ($H_{24}Mo_7N_6O_{24}\cdot 4H_2O$) was purchased from Fluka Biochemika and malachite green ($C_{23}H_{26}N_2O\cdot HCl$) from Sigma. The solutions were prepared with distilled and with 18 M (Milli-Q) deionized water. Buffer A used for enzymatic ATPase assays at neutral pH contained 40 mM Tris-HCl, pH 7.6, 10 mM $MgCl_2$, and 50 μg/mL bovine serum albumin. In the absence of salts, RepA tends to aggregate below pH 6.5 as detected by light scattering (H. Xu, unpublished results). To prevent this, buffer B used at acidic pH contained 40 mM Mes[1]/NaOH, pH 5.8, 10 mM $MgCl_2$, and 50 μg/mL bovine serum albumin, plus 60 mM NaCl. The buffers with a pH below 6.5 used for pH titration of ATPase activity studies were the same as buffer B except that Mes/NaOH was replaced by sodium acetate as indicated. Buffer C used for NTP and NDP binding tests contained 40 mM Tris-HCl, pH 7.6, and 10 mM $MgCl_2$. Gel filtration buffer contained 20 mM Tris-HCl, 150 mM NaCl, 0.1 mM EDTA, and 10% glycerol, pH 8.0.

Nucleotides and Enzymes. ϵATP, ϵADP, ATPγS, ATP, ADP, and AMP were purchased from Sigma and Amersham Corp. and used without further purification. Protein broad marker for SDS−PAGE was purchased from Boehringer Mannheim. High protein marker used for native PAGE was from Bio-Rad.

Purification of RepA Protein. The *E. coli* RSF1010 coded RepA protein was prepared and purified at 4 °C as described by Röleke et al. (*17*). The concentration of protein was determined spectrophotometrically using an extinction coefficient of $\epsilon_{280} = 25\,180\ M^{-1}\ cm^{-1}$ (monomer) (*27*). Native polyacrylamide gel electrophoresis analysis of the final purified fractions from gel filtration on Pharmacia Sephacryl S200 was run at 4 °C with 14 V/cm.

Preparation of Oligonucleotides. Oligo(dT) with 4−30 nucleotides were synthesized at the Department of Biochemistry of FU Berlin. The concentrations were determined spectrophotometrically using an extinction coefficient of $\epsilon_{260} = 8100\ M^{-1}\ cm^{-1}$ per nucleotide of oligo(dT).

ATPase Assays. ATP hydrolysis was monitored by measuring the production of inorganic phosphate using acidic ammonium molybdate and malachite green (*28*). Reactions (100 μL) were performed at 25 °C in buffer A (unless otherwise indicated). The experiments were started by the addition of RepA at a final concentration indicated (80 or 160 nM hexamer enzyme in the presence or absence of ssDNA) and stopped after 10 min with 800 μL of 3:1 (v/v) acidic malachite green/ammonium molybdate solution, followed after 1 min by addition of 100 μL of 34% (w/v) sodium citrate. After incubation for 10 min, the absorbance at 660 nm was measured using control reactions (without enzyme) as reference. All assays were performed at least in duplicate. The amount of phosphate produced was quantified using a standard curve.

Kinetic Measurements of ATPase Activity. The release rate of inorganic phosphate (P_i) versus ATP concentration (varied at least 5-fold above and below the measured K_M) was used to determine kinetic parameters. They were calculated according to the Hill equation (eq 1) with the nonlinear analysis Origin 5.0 Program.

$$\log \frac{v}{V_{max} - v} = n \log [S] - \log K_M \qquad (1)$$

where v is the rate of the hydrolysis reaction, V_{max} is the maximal rate, [S] is the concentration of ATP, and n is the Hill constant.

Inhibition measurements of ATPase activity by ATP analogues were determined by using the equation:

$$1/v = \frac{1}{V_{max}}\left[1 + \frac{K_M}{[S]}\left(1 + \frac{[I]}{K_i}\right)\right] \qquad (2)$$

where K_M and K_i are the substrate binding and inhibition constants, [S] and [I] denote the concentrations of substrate and inhibitor, and v and V_{max} are the initial and maximum velocity of the reaction, respectively.

Fluorescence Spectroscopy. Fluorescence measurements were performed using a Shimadzu RF-5000 spectrofluorometer. To avoid possible artifacts due to dilution and inner filter effects, the excitation wavelength was set at a spectral bandwidth of 3 nm and the emission bandwidth at 15 nm (*29*). Protein concentrations were adjusted as indicated and measured in cuvettes of 1 cm path length at 25 °C (unless otherwise indicated). All titration points were corrected according to the equation (*30*):

$$F_c = (F_i - F_0)(V_i/V_0)10^{0.5d(A_{iex}+A_{iem})} \qquad (3)$$

where F_c is the corrected value of the fluorescence intensity at a given point of titration, F_i is the experimentally measured fluorescence intensity, F_0 is the background, V_i is the actual

[1] Abbreviations: Mes, 4-morpholineethanesulfonic acid; ATPγS, adenosine 5′-*O*-(3-thiotriphosphate); ϵADP, 1,N^6-ethenoadenosine 5′-diphosphate.

and V_0 is the initial volume of the sample, d is the total path length of the optical cuvette (cm), A_{iex} is the absorption of the sample at the excitation wavelength, and A_{iem} is the absorption of the sample at the emission wavelength.

The binding of the fluorescent ADP analogue ϵADP was followed by monitoring the quenching of the protein tryptophan fluorescence (λ_{ex} = 300 nm; λ_{em} = 330 nm). For fluorescence titrations, protein solutions in 1 mL quartz cuvettes were titrated with aliquots of 5 mM ϵADP solution. The solutions were equilibrated for at least 0.5 h at 25 °C before titrations were initiated and stirred with a magnetic microbar after addition of ligand for about 1min. All assays were performed in duplicate. Binding constants were determined according to the equation:

$$Q = Q_1K_1/(K_1 + [L]) + Q_2K_2/(K_2 + [L]) \qquad (4)$$

where Q is the protein fluorescence quenching signal and Q_1 and Q_2 represent the maximum quenching signals of the first and second binding motifs, respectively. K_1 and K_2 are the dissociation constants of the two binding sites, and [L] denotes the total ligand concentration.

The fluorescence quenching factor of bound ligand ϵADP to RepA was determined by reverse titration of a low concentration of ligand (1.5 μM) in buffer C with an excess of enzyme (83 μM hexamer). Each titration experiment was repeated at least twice.

Circular Dichroism. CD spectra were taken at room temperature (unless otherwise indicated) with a Jasco Model 600 recording spectropolarimeter, thermostated using a constant temperature bath (Lauda). Measurements were performed in the far-UV (190−250 nm) range with 0.02 and 0.1 cm path length quartz cuvettes to avoid too high absorbance of the sample, and in the near-UV (250−320 nm) range 1 cm path length cuvettes were used. The bandwidth was 1 nm, and spectra were averaged over at least four scans in order to improve the signal-to-noise ratio. The molar ellipticity [θ] (deg·cm^2·dmol^{-1}) was calculated according to the equation [θ] = 100θ/cl, where θ is the measured ellipticity in degrees, c is the protein concentration in moles per liter, and l is the path length in centimeters. The amount of secondary structure was calculated with the commercial program SELCON3 (*31*).

Thermal Unfolding Measurements. Thermal denaturation was monitored by changes in CD spectra at 222 nm as a function of increased temperatures from 25 to 85 °C in 0.1 cm path length cuvette. Prior to taking a reading, the solutions were equilibrated for 3 min at each newly established temperature. The unfolding curve was analyzed with the nonlinear Origin Boltzmann Program to derive the melting temperature T_m and the conformational stability ΔG(25 °C) (*32*).

By assuming a two-state reversible equilibrium process between the native (F) and denatured states (U), the fraction of denatured protein f_U at temperature T was determined according to the equation $f_U = (\theta_{T,222} - \theta_F)/(\theta_U - \theta_F)$, where $\theta_{T,222}$ is the measured ellipticity at 222 nm at temperature T and θ_F and θ_U are the ellipticities at 222 nm of totally folded and unfolded states measured at 25 and 85 °C, respectively. The equilibrium constant for denaturation is obtained by using the equation $K = f_U/f_F = f_U/(1 - f_U)$. The stardard expression for the temperature dependence of ΔG is $\Delta G = -RT \ln K = -RT \ln f_U/(1 - f_U) = \Delta H - T\Delta S$; ΔS is obtained from the slope of a plot of ΔG versus T (K). Since $\Delta G = 0$ at $T = T_m$, the van't Hoff enthalpy of denaturation at T_m is $\Delta H_m = (T_m)(\Delta S_m)$. Differences in conformational stability at different experimental conditions are given by the equation $\Delta(\Delta G) = \Delta T_m \times \Delta S_m$, where ΔT_m is the difference between the T_m values and ΔS_m is the slope of ΔG versus T at T_m in kilocalories per mole per kelvin. In this text, the average slope ΔS_m calculated from all the experimental values is used.

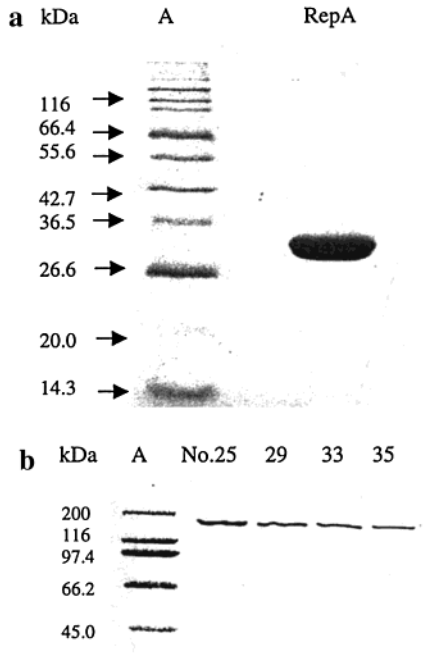

FIGURE 1: Purification of RepA protein. (a) SDS−PAGE analysis of the purified RepA protein. 1 μL of concentrated RepA (15 mg/mL) protein in gel filtration buffer was electrophoresed on an SDS−15% polyacrylamide gel (acrylamide:bisacrylamide ratio of 37.5:1), and the gel was stained with Coomassie Blue. Lane A: broad protein molecular size markers (kDa). (b) Native 10% polyacrylamide gel electrophoresis analysis of the final purified fractions (as indicated) (10 μL) in gel filtration buffer to show the formation of the hexameric protein. Lane A: high protein molecular size markers (kDa).

RESULTS

Purification of Hexameric RepA Protein. After chromatography with DEAE-Sephacel anion exchange, heparin−agarose, and gel filtration on Pharmacia Sephacryl S200, RepA is at least 95% pure as indicated by SDS−PAGE (Figure 1a). In the native gel of purified RepA only one band is observed corresponding to a protein of mass 180 kDa (Figure 1b). This suggests that the formation of the hexamer does not depend on any cofactors, such as Mg^{2+} or nucleotide, which are required by most of the other known helicases. This conclusion was also confirmed in ref *15* by the cross-linking method and further shown by the RepA crystal structure (Niedenzu et al., in preparation).

ATPase Activity and Kinetic Measurements

ssDNA Stimulates ATPase Activity. The ATPase activity of RepA does not obey classical Michaelis−Menten kinetic relationships over the ATP concentration range examined (10 μM to 1 mM), neither in the presence nor in the absence

Table 1: Steady-State Kinetic Data of RepA ATPase Activity[a]

	V_{max} (nM /s)	K_{cat} (s^{-1})	K_M (μM)	K_{cat}/K_M ($mM^{-1}\,s^{-1}$)	n
pH 5.8					
no DNA	17 ± 1	0.11 ± 0.01	48 ± 3	2.2 ± 0.2	1.60 ± 0.11
ssDNA[b]	184 ± 5	2.30 ± 0.06	173 ± 11	13.3 ± 0.9	1.82 ± 0.18
pH 7.6					
no DNA	26 ± 2	0.16 ± 0.01	69 ± 5	2.3 ± 0.2	1.71 ± 0.12
ssDNA[b]	62 ± 6	0.78 ± 0.07	96 ± 20	8.1 ± 2.2	2.34 ± 0.73

[a] K_{cat} is expressed in terms of the hexamer. [b] In the presence of 1.5 μM oligo$(dT)_{20}$.

of ssDNA. The kinetic parameters of RepA ATPase activity determined according to the Hill equation (eq 1) are shown in Table 1. The enzyme kinetic curves shown in Figure 2b are sigmoidal instead of hyperbolic as expected for a Michaelis−Menten-type mechanism. For all of the kinetic data shown in Table 1, the Hill constants for ATPase activity of RepA in the presence and absence of ssDNA are around 2, which implies positive cooperativity in sequential binding and hydrolysis of ATP.

The ATPase activity of RepA at different pH values in the range pH 4.5−8.5 has been determined in the absence and presence of ssDNA $(dT)_{20}$, as shown in Figure 2a. At pH 4.5−5.3, RepA is nearly inactive in the absence of $(dT)_{20}$ and from pH 5.3 to pH 6.0, the ATPase activity increases to a K_{cat} of 0.12 (s^{-1}); it is nearly constant from pH 6 to pH 7 and then increases again to a K_{cat} of 0.39 (s^{-1}). This contrasts the ATPase activities of RepA in the presence of $(dT)_{20}$. In the pH range considered, K_{cat} is always above 0.35 (s^{-1}) and shows an optimum ATPase in the narrow range from pH 5.3 to pH 6.0, nearly consistent with the optimal pH range for helicase (DNA unwinding) activity of RepA, which is from pH 5.5 to pH 6.0 (*15*).

Figure 2c shows stimulation of RepA ATPase activity by different $(dT)_{20}$ concentrations at pH 5.8 and 7.6. In the presence of ssDNA, the ATPase activity of RepA is much more stimulated at pH 5.8 than at pH 7.6. The amount of $(dT)_{20}$ required to achieve half-maximal ATP hydrolysis activity, K_{eff}, is 65 nM at pH 5.8, while at pH 7.6, there is a nearly linear relationship so that saturation could not be observed.

Length of ssDNA Required for Optimal ATPase Activity. The requirement for ssDNA stimulated ATPase activity was further studied by adding oligo(dT) from 4 to 30 nucleotides in buffer B, 25 °C (Table 2). The results show that the ATPase activity of RepA is stimulated by ssDNA with 6 or more nucleotides, but K_{eff} is dramatically increased if the length of the oligonucleotides is shorter than a 10mer, indicating that longer oligonucleotides (>10mer) bind more tightly.

Inhibition of RepA ATPase Activity by ATP Analogues. Since RepA hydrolyzes ATP even in the absence of ssDNA at 25 °C, nonhydrolyzable analogues were used to study the properties of nucleoside tri- and diphosphates binding to the enzyme. The ability of ATPγS, ϵADP, ADP + AlF_3, ADP, and AMP to compete with ATP for the enzyme active site was examined using eq 2 (see Materials and Methods). Similar competitive inhibitory effects were observed for ATPγS (Figure 3), ϵADP, ADP, and ADP + AlF_3. ATPγS is the strongest inhibitor, with a K_i of 97.5 μM (Table 3). AMP does not show any significant inhibitory effect under these conditions, indicating that β- and γ-phosphates have an important role in ATP binding.

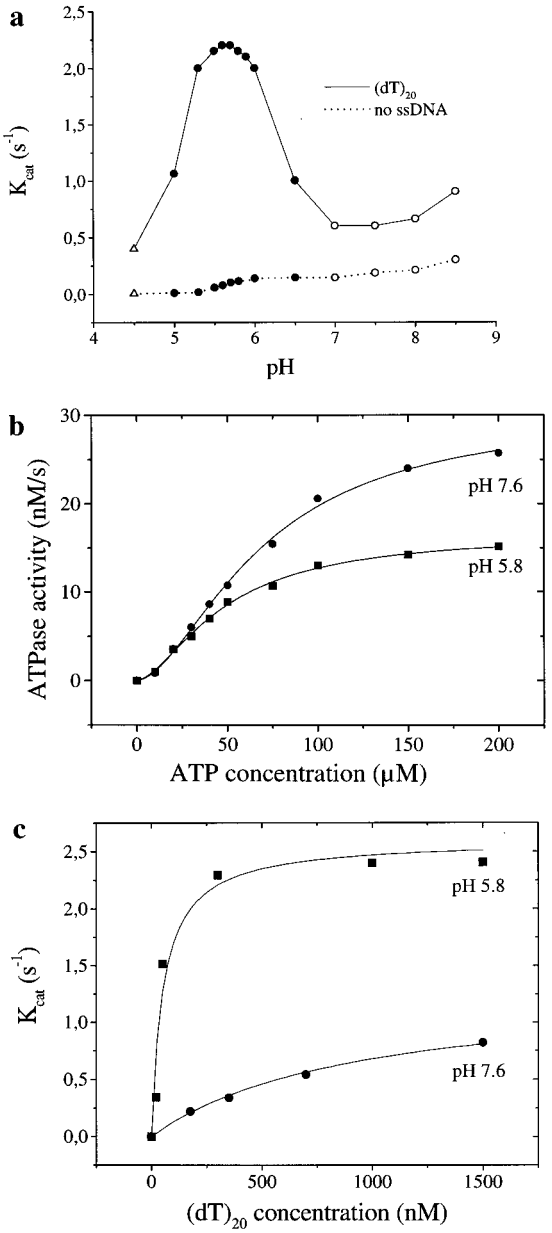

FIGURE 2: ATPase activity of RepA depends on pH and is stimulated by ssDNA. (a) pH titration of ATPase activity of RepA at 25 °C in the presence (—) and absence (· · ·) of 700 nM $(dT)_{20}$: (△) 40 mM sodium acetate; (●) 40 mM Mes/NaOH; (○) 40 mM Tris-HCl. (b) ATPase activity of RepA in the absence of ssDNA. The hydrolysis of ATP by RepA was measured under steady-state conditions at 25 °C as described under Materials and Methods using RepA, 160 nM (hexamer), and ATP (10−200 μM). The rate of ATP hydrolysis, V (nM/s), is plotted versus the concentration of ATP, and the curve was analyzed according to the Hill equation to obtain values for K_{cat}, K_M, and the Hill constant n; see Table 1. Plots: (●) in buffer A, pH 7.6; (■) in buffer B, pH 5.8. (c) Stimulation of ATPase activity by ssDNA, $(dT)_{20}$. Rates of ATP hydrolysis were determined at various concentrations of $(dT)_{20}$ in the presence of saturating quantities of ATP as described in Materials and Methods using 80 nM RepA (hexamer). The data points represent the average of at least two experiments. Plots: (●) pH 7.6; (■) pH 5.8.

Fluorescence Measurements on ϵADP Binding to RepA

Interaction of Etheno Nucleotides with RepA. In the presence of etheno-modified ATP and ADP, there is a

Table 2: Relationship between Oligonucleotide Length and Steady-State Rate[a] and K_{eff}[a]

ssDNA	steady-state rate (s^{-1})	K_{eff} (nM)
$(dT)_4$	0.95 ± 0.04[b]	ND[c]
$(dT)_6$	2.34 ± 0.18	2651 ± 763
$(dT)_8$	2.38 ± 0.38	2053 ± 789
$(dT)_9$	2.19 ± 0.40	1008 ± 406
$(dT)_{10}$	2.29 ± 0.33	240 ± 171
$(dT)_{20}$	2.22 ± 0.16	65.1 ± 34.4
$(dT)_{30}$	2.39 ± 0.16	63.4 ± 30.1

[a] K_{eff} [the amount of $(dT)_n$ to achieve half-maximal ATPase activity] and steady-state rate were determined by analyzing the dependence of the ATPase activity on different concentrations of oligonucleotides $(dT)_n$ at 1 mM ATP. The data were analyzed by plotting $1/K_{cat}$ against 1/[ssDNA]. [b] Measured at an oligonucleotide concentration of 39 μM. [c] Cannot be determined.

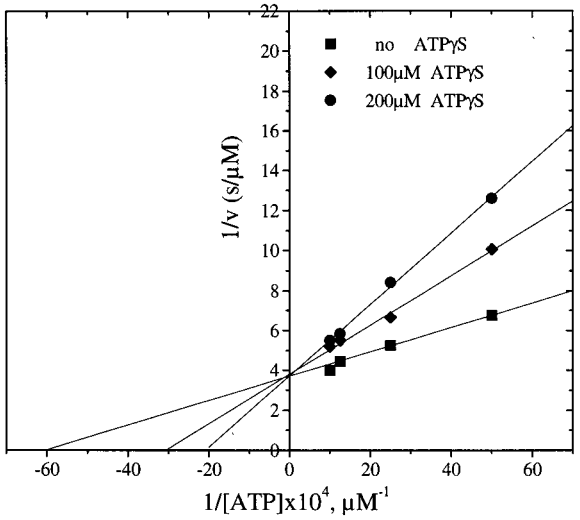

FIGURE 3: Double-reciprocal Lineweaver−Burk plots describing the inhibition of ATPase activity of RepA by ATPγS. The assays were carried out as described in Materials and Methods except that ATPγS was added in the amount indicated at each data point to reaction mixtures containing varying amounts of ATP, and after 10 min the amount of produced P_i was determined, yielding the rates v (see Materials and Methods of determining K_M and K_i). RepA is 80 nM (hexamer) in the presence of 700 nM $(dT)_{20}$ in buffer B, pH 5.8.

Table 3: Determination of Inhibition (K_i) of RepA ATPase Activity by Different ATP Analogues[a]

nucleotide	K_M (μM)	K_i (μM)
ATP	150	
ATPγS		97.5
ADP + AlF_3		102[b]
ADP		120
ϵADP		135
AMP		>1000

[a] RepA is 80 nM (hexamer) in the presence of 700 nM $(dT)_{20}$ in buffer B, pH 5.8. [b] The molar ratio ADP:AlF_3 = 1. The aluminum fluoride minics an oxygen-bound phosphate when complexed with the protein (*33*).

significant overlap of the absorption spectra of the ATP analogues with the protein tryptophan fluorescence emission spectrum, giving rise to energy transfer between tryptophan and nucleotide and quenching of the protein fluoresence (*34*). This effect was used to monitor the binding of such nucleotides to RepA. Figure 4a shows the titration curves of fluorescence quenching as a function of ϵADP concentration.

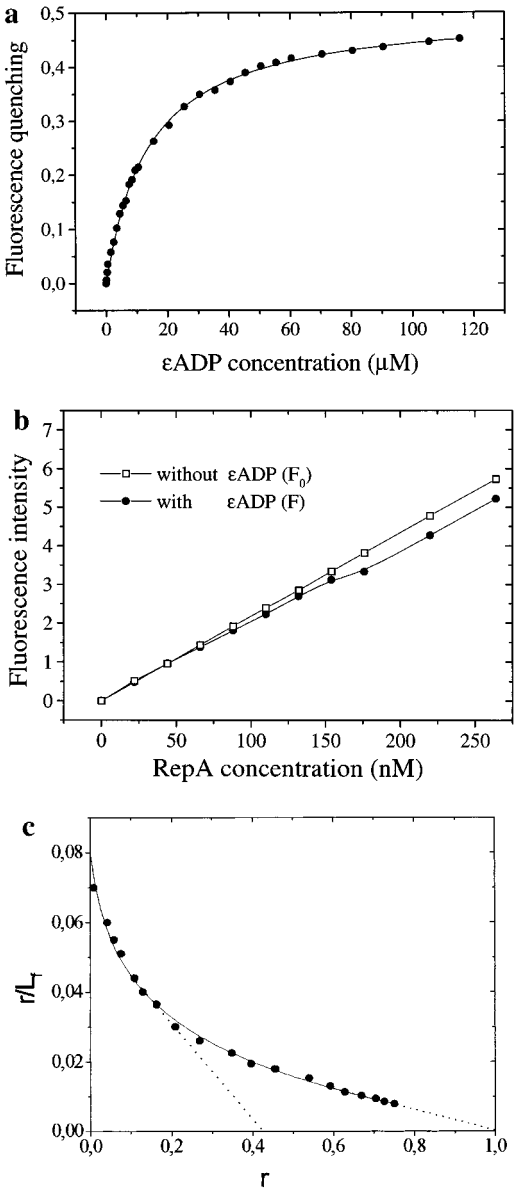

FIGURE 4: Fluorescence titration studies on binding of ϵADP to the RepA hexamer. (a) Fluorescence titration of binding of ϵADP to the RepA hexamer in buffer C at 25 °C. The measurement was monitored by the quenching of the intrinsic protein fluorescence at λ_{ex} = 300 nm and λ_{em} = 330 nm. The RepA concentration is 5 μM (monomer). (b) Reverse fluorescence titration to determine the fluorescence quenching factor of bound ligand to protein: (●) and (□), the titration curves of fluorescence intensity quenched in the presence and absence of 1.5 μM ϵADP in buffer C, repectively, at 25 °C. The RepA concentration is indicated as a hexamer. The calculated fluoresence quenching factor is 0.08 ± 0.02 μM^{-1} (see text). (c) Scatchard plot for the fluorescence titration of ϵADP binding to RepA in buffer C. r denotes the concentration ratio of bound ligand to protein (monomer). L_f denotes free ligand concentration. Measurement was done at 25 °C and RepA, 12.0 μM (monomer).

To determine whether the tryptophan fluorescence quenching of RepA is exclusively caused by the binding of ϵADP at the active site, the fluorescence of helicase was also measured in the absence of Mg^{2+}. Since ATP and its analogues do not bind to the active site of RepA without Mg^{2+}, nearly no fluorescence quenching of RepA occurs. A variant of this study is that, after titration with ϵADP in buffer C, the formed complex is back-titrated with ATP. This was performed at 4 °C in the absence of ssDNA since the ATPase

catalytic turnover is nearly undetectable under these conditions and ATP only binds to RepA but is not hydrolyzed. Addition of ATP results in a reversal of fluorescence quenching (data not shown), indicating that ϵADP binds to the active site of RepA.

Stoichiometry of Nucleotide Binding Sites in RepA. Reverse titration was used to study the number of ϵADP binding sites per RepA hexamer in the absence of ssDNA. In Figure 4b, 1.5 μM ϵADP was titrated with 83 μM RepA (hexamer) in buffer C at 25 °C. The determined fluorescence quenching factor $Q = (F_0 - F)/(F_0[L]) = 0.08 \pm 0.02\ \mu M^{-1}$, where F and F_0 are the fluorescence intensities in the presence and absence of ϵADP, respectively, when 1.5 μM ϵADP is totally bound to RepA, and [L] is the total ϵADP concentration.

According to the calculated fluorescence quenching factor, a typical Scatchard plot was constructed from the titration of ϵADP to 12.0 μM RepA (monomer) in buffer C as displayed in Figure 4c. The Scatchard plot is biphasic rather than linear, indicating that the RepA hexamer contains two types of ATP binding sites differing in affinity or that there are negative cooperative interactions between binding sites. Extrapolation of the curves to the abscissa yields $r = 0.4$ and $r = 1.0$; i.e., the maximum number of ϵADP binding sites per RepA monomer is one, or six ϵADP are bound per hexamer.

It should be noted that the quenching of tryptophan fluorescence caused by the binding of ϵADP may not be linear in the coverage of sites (*35*). It is possible that binding of the first three ligands quenches more than half of the fluorescence of the protein especially when the quenching effect occurs across the subunit interface (*36*). Moreover, the average energy transfer efficiency may depend nonlinearly on the average number of bound ϵADP/RepA hexamer, being higher at the high-affinity sites and lower at the low-affinity sites, as also observed for DnaB helicase (*37*). As a consequence, the limiting slope and extrapolated stoichiometric relationship of the first strong binding sites in the Scatchard plot (Figure 4c) are smaller than half if three strong and three weak binding sites are expected, especially at low protein concentration (data not shown).

From the Scatchard plot alone (Figure 4c), it is difficult to distinguish between the two possibilities—two different binding sites or negative cooperativity among the binding sites depending on which model is considered on the basis of parsimony and symmetry of the known structure information. For the structure of hexameric helicase DnaB showing negative cooperativity, two models with hexagon and octahedron symmetry were proposed (*24*). The hexagon model was preferred since negative cooperative interactions are limited to or predominant between nearest neighbor sites. We adopt here the view that RepA has three strong and three weak binding sites in the absence of ssDNA for the reason that some hexameric helicases, such as Rho and DnaB, can function as a trimer of dimers; for some other helicases, such as bacteriophage T7 DNA helicase, the weak nucleotide binding sites are hardly detectable so that only three strong nucleotide binding sites are found (*26*).

Determination of the Binding Constants. If we assume a model with six ATP binding sites per RepA hexamer divided into two classes containing three strong and three weak sites as described previouly, a simple nonlinear binding isotherm can be formulated (eq 4) and used to model the two binding sites (see Materials and Methods). The ϵADP binding (Figure 4a) corresponds very well to this equation. In the absence of ssDNA, the fit yields strong affinity binding site(s), $K_1 = 1/K_1 = 1.54 \pm 0.31 \times 10^6\ (M^{-1})$, and weak binding site(s), $K_2 = 1/K_2 = 4.71 \pm 0.23 \times 10^4\ (M^{-1})$, which differ by 30−40-fold.

Circlar Dichroism Studies on Nucleotide Binding

In the presence of 60 mM NaCl, the far-UV CD spectrum (190−260 nm) of RepA (10 μM monomer) remains essentially constant from pH 7.6 to pH 5.8 (data not shown). The commercial program (SELCON3) analyzing the spectra in terms of secondary structure shows that RepA contains 30.6% α-helix, 20% β-strands, and 49.4% random folds, consistent with the X-ray structure of RepA, which shows 26.6% α-helix, 19.4% β-strands, and 54% random folds (Niedenzu et al., in preparation).

Figure 5 shows the far-UV and the near-UV region CD spectra analyzing the secondary and tertiary structures of RepA upon binding of ATPγS. The CD spectrum in the peptide region of RepA remains totally unchanged upon addition of a 2-fold excess of ATPγS (Figure 5a). ATPγS itself has a negligible CD signal in this region compared to the peptide signal as a result of the high α-helix content of RepA. Further addition of 100 μM ATPγS still does not significantly change the CD spectrum of RepA, suggesting that its polypeptide backbone is unaffected by the binding of ATPγS at these experimental conditions.

Figure 5b shows the CD spectra of RepA with and without ATPγS in the near-UV region (250−320 nm). The corresponding spectrum of free ATPγS is also shown. The spectrum of the mixture (RepA + ATPγS) is clearly different from the sum of the spectra of the free components. In the difference spectrum shown in Figure 5c, a negative CD spectral change is observed for RepA upon binding of ATPγS. Since the CD signal in the near-UV wavelength region is due to electronic transitions of the aromatic residues of the protein or/and of the adenine base of the cofactor, the negative CD spectral change indicates a variation in enviroment of aromatic groups of RepA upon binding of ATPγS, suggesting tertiary structure changes. This is consistent with the recently determined X-ray structure of RepA showing that the adenine−ribose moiety of ATP is located in a cleft formed between adjacent monomers, with the adenine base stacked between Arg254 of the same and Tyr243 of the adjacent monomer.

Thermal Unfolding of RepA in the Absence and Presence of ATPγS and ADP. The thermal unfolding of RepA was studied in the range from 25 to 85 °C in buffer C by recording far-UV CD spectra as a function of temperature (Figure 6a) and CD ellipticity changes at 222 nm. The thermal unfolding pathway of RepA follows a simple two-state mechanism and is irreversible.

The thermal stability of RepA was also studied in the presence of nucleotides. Figure 6b shows that the nonhydrolyzable ATPγS increases the melting temperature of RepA by 2.30 °C at pH 7.6, corresponding to an increase in thermal stability $\Delta(\Delta G)$ of 0.95 kcal/mol (Table 4), whereas binding of ADP increases the T_m by only 0.70 °C, corresponding to 0.29 kcal/mol.

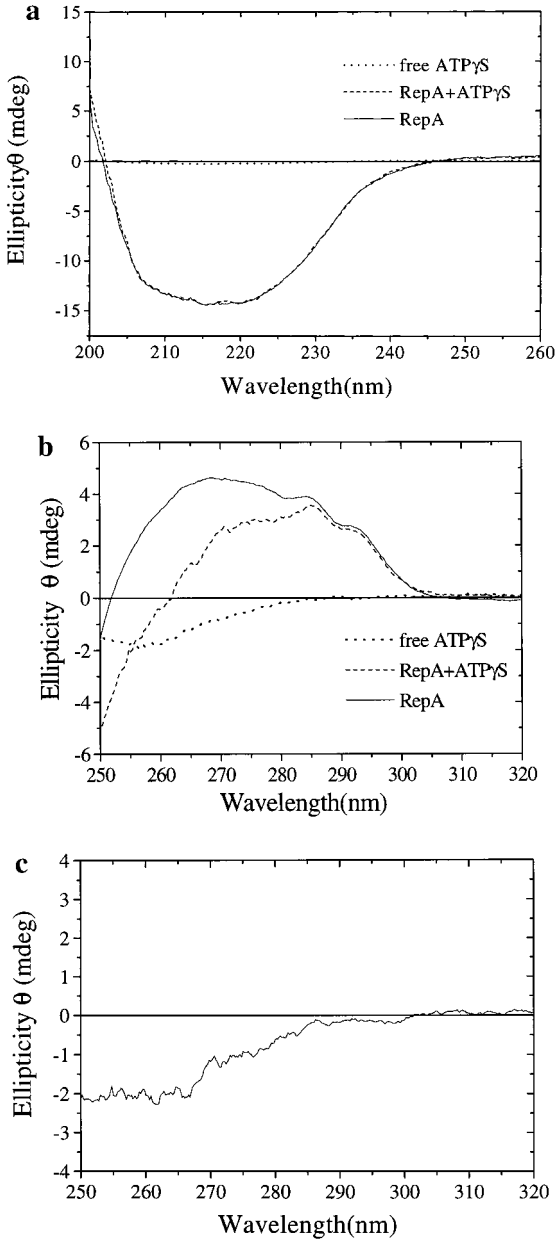

FIGURE 5: Circular dichroism spectra in the far- and near-UV region of RepA with and without ATPγS. (a) Far-UV region (200−260 nm): 10 μM RepA (monomer) in the presence (- - -) and absence (—) of 20 μM ATPγS, as well as the spectrum for 20 μM ATPγS in the absence of RepA (• • •) in buffer C, pH 7.6. (b) Near-UV region (250−320 nm) CD spectra in buffer C, pH 7.6. 30 μM RepA (monomer) with (- - -) and without (—) 60 μM ATPγS and the spectrum of free 60 μM ATPγS in the absence of RepA (• • •). (c) Difference CD spectrum between the RepA−ATPγS complex and the sum of the separate CD spectra of ATPγS and RepA solutions. For far-UV and near-UV CD measurement, cell path lengths were 0.1 cm and 1 cm, respectively.

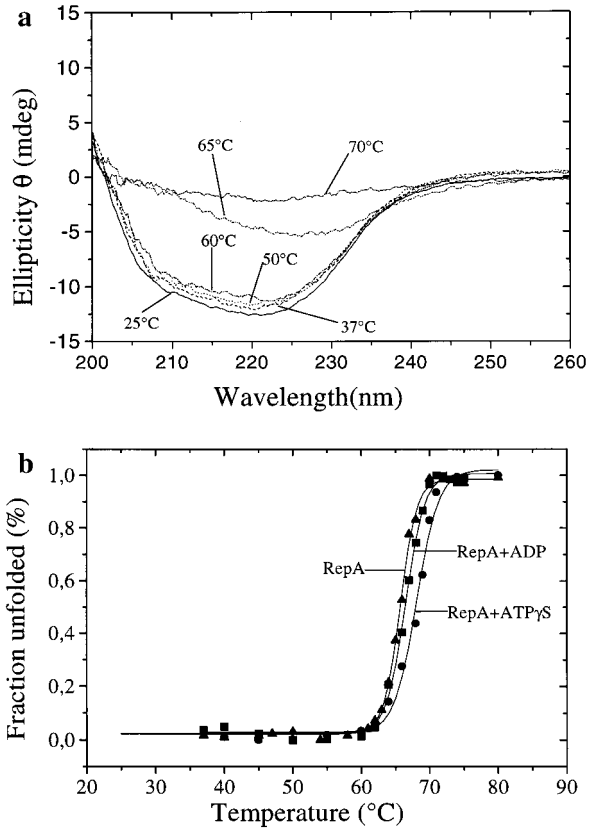

FIGURE 6: Thermal-induced unfolding and stability of RepA. The RepA concentration was 5 μM (monomer) and the cell path length was 0.1 cm. (a) Far-UV region CD spectra measured at different temperatures in buffer C, pH 7.6. (b) Thermal unfolding curves of RepA in the absence (▲) and presence of ATPγS (●) and ADP (■) in buffer C, pH 7.6. ATPγS and ADP concentrations were 250 μM. The unfolded fraction of RepA was obtained from ellipticity changes at 222 nm as described in Materials and Methods.

Table 4: Parameters Characterizing the Thermal Unfolding and Stability of RepA[a]

	T_m[b] (°C)	ΔT_m[c] (°C)	ΔS_m[d] [kcal/(mol K)]	ΔH_m[e] (kcal/mol)	$\Delta(\Delta G)$[f] (kcal/mol)
RepA	65.8 ± 0.1		0.412	139.6	
RepA + ATPγS	68.1 ± 0.2	2.3 ± 0.2	0.412	140.5	0.95 ± 0.08
RepA + ADP	66.5 ± 0.1	0.7 ± 0.1	0.412	139.9	0.29 ± 0.05

[a] The RepA concentration is 5 μM (monomer) and ATPγS and ADP concentrations are 250 μM, in 40 mM Tris-HCl and 10 mM $MgCl_2$, pH 7.6. The cuvette path length is 0.1 cm. [b] T_m is the midpoint of the thermal unfolding curve in °C. [c] ΔT_m is the difference between the T_m values. [d] ΔS_m is the slope of ΔG versus T at T_m in kcal/(mol K). In this column, the average slope ΔS_m calculated from all the experimental values is used. [e] $\Delta H_m = T_m(K) \times \Delta S_m$ in kcal/mol. [f] $\Delta(\Delta G) = \Delta T_m(K) \times \Delta S_m$, where ΔS_m is the average experimental value.

DISCUSSION

NTP binding and hydrolysis is crucial for DNA unwinding by helicases. This is shown by several reported helicase variants deficient in ATP binding and hydrolysis which have only weak helicase activity (*38*, *39*). In the present report on RepA, the steady-state kinetic parameters of ATPase activity were studied in the presence and absence of ssDNA, and fluorescence titrations and CD spectroscopy were applied to elucidate the properties of nucleotide binding to RepA.

From the recently determined X-ray structure of RepA, we know that the "Walker A" motif of RepA contains a glycine-rich segment including the sequence ^{40}Gly-Ala-Gly-Lys-Ser^{44}. Model building has shown that the lysine may bind to the β- and γ-phosphates of ATP while the adenine−ribose moiety of ATP is located in a cleft formed between adjacent monomers. The adenine base is found sandwiched between Arg254 of the same (in cis) and Tyr243 of the adjacent (in trans) monomer. In studies with different hydrolyzable nucleoside triphosphates, Scherzinger et al. (*15*) showed that RepA has a requirement for purine nucle-

otides: ATP, dATP, GTP, and dGTP support helicase action, while CTP, dCTP, UTP, and dTTP are poor cofactors. This suggests that pyrimidine-based nucleoside triphosphates may bind to RepA with low affinity, and they also exhibit low hydrolysis activity, probably because the interaction between pyrimidine bases and the side chains of Tyr243 and Arg254 is weak or the pyrimidine bases are poorly accommodated within the binding pocket compared to adenine or guanine. Although modified on the adenine residue, ϵATP can also be hydrolyzed by RepA with $K_{cat} = 0.05\ s^{-1}$ at pH 7.6, 25 °C, in the absence of ssDNA (data not shown), and the tight binding of ϵADP to RepA (Table 3) indicates that this modified etheno base may interact with Tyr243 and Arg254 without steric interference, as also suggested by the X-ray structure.

As the NTP binding sites in RepA are located at the interfaces between adjacent monomers, this configuration may facilitate conformational changes transferred to neighboring subunits upon NTP binding and hydrolysis. It is possible that the binding of an NTP molecule to the interface between two monomers causes conformational changes that are communicated to the adjacent subunit, resulting in a decrease of the binding affinity for NTP to the second subunit interface. This could give rise to high-affinity and low-affinity binding sites adjacent to each other in the RepA hexamer.

Thermal unfolding studies show that binding of ATPγS and ADP to RepA indeed stabilizes interunit contacts of the two monomers. In the presence of ATPγS, RepA is more stable (+2.3 °C) than in the presence of ADP (+0.7 °C, Table 4), compared to free RepA. This finding suggests that the γ-phosphate of ATP contributes additional contacts that stabilize the structure of RepA, in contrast to ADP where this phosphate is missing.

ATP hydrolysis by RepA shows positive cooperativity in both the absence and presence of ssDNA (Table 1). Here we propose a model in which individual subunits of RepA sequentially and cooperatively perform a multistep ATP hydrolytic cycle in the absence of ssDNA (Figure 7). We assume that the ATP binding sites of RepA can exist in either of two conformational states, R (relaxed), when the site is filled by ADP and inorganic phosphate, P*i*, and T (tense), when it is filled by ATP. We also assume that the transition from R to T forms occurs sequentially. During the hydrolysis reaction, ATP bound at three strong affinity sites (form T) of RepA is hydrolyzed, and the three strong ATP binding sites are now occupied by ADP and inorganic phosphate, P_i; RepA undergoes a conformational change, with the ATP binding sites changing from T to R form and vice versa. Since the ATPase active site and adenine binding site are formed by adjacent subunits, conformational changes may be easily transmitted to neighboring subunits such that the weak binding sites become strong ATP binding sites (from R to T form). They bind and hydrolyze ATP again, and the cycle continues.

In the presence of ssDNA, this scheme becomes more complicated. It has been suggested that ssDNA passes through the central hole of the hexameric ring formed by the *E. coli* RuvB helicase (*9*), the bacteriophage T7 gp4 helicase (*8*), SV40 large T antigen (*40*), and the *E. coli* DnaB helicase (*41*). The X-ray structure of RepA indicates that only ssDNA can pass through the 17 Å diameter central hole of the hexamer. It has been suggested that ssDNA binds

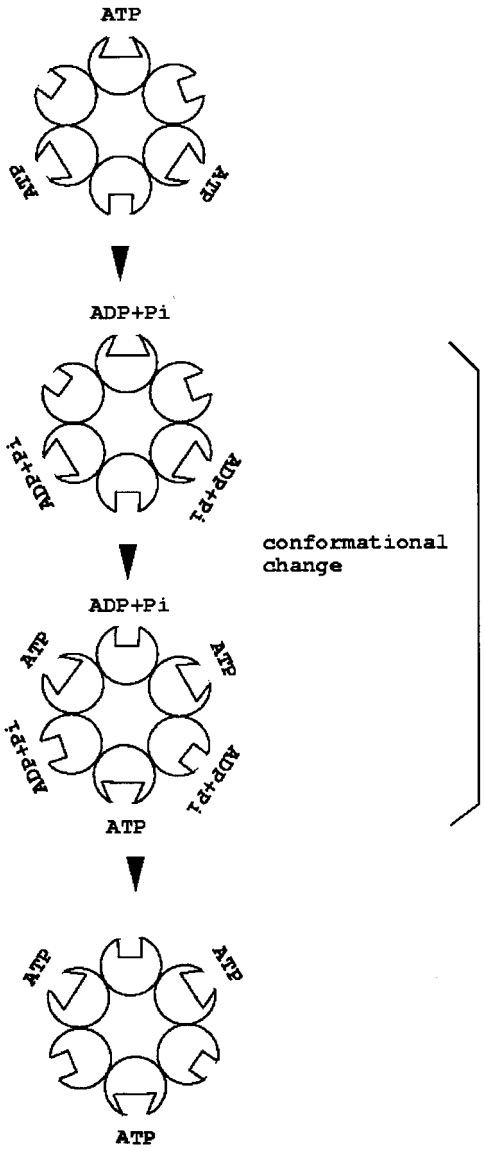

FIGURE 7: Scheme of steps in the ATP hydrolysis pathway of RepA in the absence of ssDNA. The catalytic sites are differentiated as tight forms (T forms, triangle shape) which bind ATP or relaxed forms (R forms, rectangle shape) which are filled with ADP + P_i.

tightly to only one or two subunits of the hexameric helicases (*8*, *41*, *42*). This may be required for dsDNA unwinding where each subunit or pair of subunits of RepA alternately participates in ssDNA binding and release reactions (*42*, *43*). Such an asymmetric pattern can also generate nonequivalent NTP hydrolysis active sites in a multisubunit enzyme so that only one or two of the six subunits are engaged in NTP hydrolysis at each unwinding cycle, and they sequentially bind and hydrolyze NTPs at the catalytic sites with positive cooperativity (*44*−*46*). This is similar to F_1-ATPase (*47*, *48*), because the γ-subunit of F_1-ATPase is positioned within the central cavity of the hexameric ring of α- and β-subunits, analogous to the way in which the hexameric helicases bind ssDNA (*49*).

RepA shows optimal dsDNA unwinding activity at pH5.6, while at pH 7.6, only 20% of the unwinding activity remains (*15*). In the present study, we found ssDNA to stimulate ATPase activity of RepA much more at acidic pH (5.3−6.0) than at pH 7.6. This might be the reason RepA unwinds dsDNA optimally only in the narrow acidic pH range 5.5−

6.0. Fluorescence correlation spectroscopy has further shown that between pH 5.5 and pH 6.0 in the presence of ATPγS the binding of ssDNA to RepA is optimal, while at pH 7.6, the binding affinity is so weak that it is difficult to monitor formation of the helicase−DNA complex (Xu et al., in preparation). Such a low optimal pH may lead to reduced enzymatic activity at physiological pH, which was also reported for yeast *Saccharomyces cerevisiae* RAD3 helicase (*16*). There is a strict correlation between optimal ssDNA binding at acidic pH to RepA and stimulation of ATPase activity which drives efficient unwinding of dsDNA. This protocol will permit the screening of putative in vivo helicase inhibitor compounds by monitoring the ATPase activity in the presence of ssDNA.

Unlike the principal *E. coli* replication protein DnaB, which needs the DnaG primase to function as a mobile promoter for primer synthesis, RepA helicase does not interact with RepB' primase either in unwinding reactions or in primer synthesis assay. The 3' single-stranded tail like the "preformed replication fork" found necessary for other helicases, such as DnaB, phage T4 gene 41, and bacteriophage T7 gp4 protein, is not essential for RepA (*15*). The finding that RepA requires at least a decanucleotide as cofactor to stimulate ATPase activity provides clues for the importance of the interaction between RepA and ssDNA and suggests that it is the minimum length of single-stranded DNA in the template strand that will enable RepA helicase to bind and initiate unwinding of duplex DNA. It still remains to be elucidated how DNA interacts with RepA since this will be important for understanding the mechanism of the unwinding reaction.

ACKNOWLEDGMENT

We thank Dr. Werner Schröder for oligonucleotide synthesis and Dr. Yannis Georgalis for help with CD and fluorescence spectroscopy measurements.

REFERENCES

1. Matson, S. W., and Kaiser-Rogers, K. A. (1990) *Annu. Rev. Biochem.* 59, 289−329.
2. Lohman, T. M., and Bjornson, K. P. (1996) *Annu. Rev. Biochem. 65*, 169−214.
3. Hanawalt, P. C. (1994) *Science 266*, 1957−1958.
4. Friedberg, E. C. (1992) *Cell 71*, 887−889.
5. Yu, C.-E., and Schellenberg, G. D. (1996) *Science 272*, 258−262.
6. San Martin, M. C., Stamford, N. P. J., Dammerova, N., Dixon, N. E., and Carazo, J. M. (1995) *J. Struct. Biol. 114*, 167−176.
7. Yu, X., Jezewska, M. J., Bujalowski, W., and Egelman, E. H. (1996) *J. Mol. Biol. 259*, 7−14.
8. Egelman, E. H., Yu, X., Wild, R., Hingorani, M. M., and Patel, S. S. (1995) *Proc. Natl. Acad. Sci. U.S.A. 92*, 3869−3873.
9. Stasiak, A., et al. (1994) *Proc. Natl. Acad. Sci. U.S.A. 91*, 7618−7622.
10. Gogol, E. P., Seifried, S. E., and von Hippel, P. H. (1991) *J. Mol. Biol. 221*, 1127−1138.
11. Wong, I., and Lohman, T. M. (1992) *Science 256*, 350−355.
12. Runyon, G. T., Wong, I., and Lohman, T. M. (1993) *Biochemistry 32*, 602−612.
13. Scholz, P., Haring, V., Wittman-Liebold, B., Ashman, K., Bagdasarian, M., and Scherzinger, E. (1989) *Gene 75*, 271−288.
14. Scherzinger, E., Haring, V., Lurz, R., and Otto, S. (1991) *Nucleic Acids Res. 19*, 1203−1211.
15. Scherzinger, E., Ziegelin, G., Barcena, M., Carazo, J. M., Lurz, R., and Lanka, E. (1997) *J. Biol. Chem. 272*, 30228−30236.
16. Sung, P., Higgins, D., Prakash, L., and Prakash, S. (1988) *EMBO J. 7*, 3263−3269.
17. Röleke, D., Hoier, H., Bartsch, C., Umbach, P., Scherzinger, E., Lurz, R., and Saenger, W. (1997) *Acta Crystallogr., Sect. D 53*, 213−216.
18. Fass, D., Bogden, C. E., and Berger, J. M. (1999) *Structure 7*, 691−698.
19. Sawaya, M. R., Guo, S., Tabor, S., Richardson, C. C., and Ellenberger, T. (1999) *Cell 99*, 167−177.
20. Saraste, M., Sibbald, P. R., and Wittinghofer, A. (1990) *Trends Biochem. Sci. 11*, 430−434.
21. Walker, J. E., Sarsate, M., Runswick, M. J., and Gay, N. J. (1982) *EMBO J. 1*, 945−951.
22. Schulz, G. E. (1992) *Curr. Opin. Struct. Biol. 2*, 61−67.
23. Wong, I., Chao, K. L., Bujalowski, W., and Lohman, T. M. (1992) *J. Biol. Chem. 267*, 7596−7610.
24. Bujalowski, W., and Klonowska, M. M. (1993) *Biochemistry 32*, 5888−5900.
25. Geiselmann, J., and von Hippel, P. H. (1992) *Protein Sci. 1*, 850−860.
26. Hingorani, M. M., and Patel, S. S. (1996) *Biochemistry 35*, 2218−2228.
27. Niedenzu, T. (1997) Diploma Thesis, Fachbereich Chemie der Freien Universität Berlin.
28. Lanzetta, P. A., Alvarez, L. J., Reinach, P. S., and Candia, O. A. (1979) *Anal. Biochem. 100*, 95−97.
29. Parker, C. A. (1968) *Photoluminescence of Solutions*, Elsevier Publishing Co., Amsterdam.
30. Lakowicz, J. R. (1983) *Principle of Fluorescence Spectroscopy*, Chapter 10, Plenum Press, New York.
31. Sreerama, N., et al. (1993) *Anal. Biochem. 209*, 32−44.
32. Pace, C. N., Shirley, B. A., and Thomson, J. A. (1986) *Methods Enzymol. 131*, 311−330.
33. Wittinghofer, A. (1997) *Curr. Biol. 7*, R682−R685.
34. Eftink, M. R., and Ghiron, C. A. (1981) *Anal. Biochem. 114*, 199−227.
35. Halfman, C. J., and Nishida, T. (1972) *Biochemistry 11*, 3493−3498.
36. Eftink, M. R. (1997) *Fluorescence Spectrosc. 11*, 221−257.
37. Bujalowski, W., and Klonowska, M. M. (1994) *J. Biol. Chem. 269*, 31359−31371.
38. Hall, M. C., and Matson, S. W. (1997) *J. Biol. Chem. 272*, 18614−18620.
39. Brosh, R. M., Jr., and Matson, S. W. (1995) *J. Bacteriol. 177*, 5612−5621.
40. Dean, F. B., Borowiec, J. A., Eki, T., and Hurwitz, J. (1992) *J. Biol. Chem. 267*, 14129−14137.
41. Bujalowski, W., and Jezewska, M. J. (1995) *Biochemistry 34*, 8513−8519.
42. Yu, X., Hingorani, M. M., Patel, S. S., and Egelman, E. H. (1996) *Nat. Struct. Biol. 3*, 740−743.
43. Biswas, E. E., and Biswas, S. B. (1999) *Biochemistry 38*, 10929−10939.
44. Hingorani, M. M., Washington, M. T., Moore, K. C., and Patel, S. S. (1997) *Proc. Natl. Acad. Sci. U.S.A. 94*, 5012−5017.
45. Marrione, P. E., and Cox, M. M. (1995) *Biochemistry 34*, 9809−9818.
46. Marrione, P. E., and Cox, M. M. (1996) *Biochemistry 35*, 11228−11238.
47. Washington, M. T., Rosenberg, A. H., Griffin, K., Studier, F. W., and Patel, S. S. (1996) *J. Biol. Chem. 271*, 26825−26834.
48. Abrahams, J. P., Leslie, A. G. W., Lutter, R., and Walker, J. E. (1994) *Nature 370*, 621−628.
49. West, S. C. (1996) *Nature 384*, 316−317.

BI0008938